

# The 3 August 2009 $M_w$ 6.9 Canal de Ballenas Region, Gulf of California, Earthquake and Its Aftershocks

by Raúl R. Castro, Carlos Valdés-González, Peter Shearer, Victor Wong, Luciana Astiz,  
Frank Vernon, Arturo Pérez-Vertti, and Antonio Mendoza

**Abstract** On 3 August 2009 an earthquake of magnitude  $M_w$  6.9 occurred near Canal de Ballenas, in the north-central region of the Gulf of California, Mexico. The focal mechanism of the main event, reported in the Global Centroid Moment Tensor (CMT) catalog, is right lateral strike-slip with a strike of  $216^\circ$  and a dip of  $78^\circ$ . The initial location reported by the National Seismological Service of Mexico [Servicio Sismológico Nacional (SSN)] and the Array Network Facility (ANF) suggested that the epicenter was on the North American plate near the Tiburón fault, which is considered inactive. This earthquake was preceded by a magnitude  $m_b$  5.5 event that occurred about 5 min before. In the next 40 min after the main event two aftershocks with magnitudes  $m_b$  4.9 and  $M_w$  6.2 occurred, and on 5 August a third aftershock of  $M_w$  5.7 was located in the Canal de Ballenas region. The events of August 2009 were recorded by the regional stations of the broadband network Red Sismológica de Banda Ancha (RESBAN) that Centro de Investigación Científica y de Educación Superior de Ensenada (CICESE) operates and by stations of the SSN also located in the region of the Gulf of California. We used body-wave arrivals to determine precise epicentral locations and to estimate the rupture area of this important sequence of earthquakes. The resulting hypocentral coordinates indicate that the main event of this sequence occurred along the Canal de Ballenas transform fault, with a rupture length of 50 km. Based on the aftershock distribution, we estimate that the main event had a rupture area of approximately  $600 \text{ km}^2$ , an average slip of 1.3 m, and a stress drop of 2.2 MPa.

## Introduction

The Gulf of California, Mexico (GoC hereafter) is an oblique rift system with short spreading segments connected by long transform faults (Lonsdale, 1989; Lizarralde *et al.*, 2007). Most earthquakes in the GoC result from the relative motion of the Pacific and North American plates (Molnar, 1973). The transform faults between the Delfin ( $\sim 30.2^\circ \text{ N}$ ,  $113.8^\circ \text{ W}$ ) and Carmen ( $\sim 26.5^\circ \text{ N}$ ,  $110.2^\circ \text{ W}$ ) basins have been the site of most of the plate boundary earthquakes with  $M_s > 6$  (Goff *et al.*, 1987). In particular, along the transform fault of Canal de Ballenas, in the north-central region of the GoC (Fig. 1), several important earthquakes have occurred in the past (Fig. 2). For instance, on 8 July 1975 an event with  $M_s$  6.5 occurred west of the island Angel de la Guarda (Munguía *et al.*, 1977). Moderate magnitude earthquakes have also occurred in this region to the north, in the lower Delfin basin, on 26 November 1997 ( $M$  5.5) and south of Angel de la Guarda island on 12 November 2003 ( $M_w$  5.4) and 24 September 2004 ( $M_w$  5.8). The Angel de la Guarda earthquake of 12 November 2003 triggered seismicity on the Canal de Ballenas fault as well as on a

normal fault located west of the island. This event was preceded by a foreshock of  $M_w$  4.4 (Rodríguez-Lozoya *et al.*, 2008). The Global Centroid Moment Tensor (CMT) catalog lists 17 earthquakes with moment magnitudes  $5.2 \leq M_w \leq 6.9$  in this region between 1976 and 2009. We plotted these events in Figure 2, together with the focal mechanism determined by Munguía *et al.* (1977) for the July 1975 ( $M_s$  6.5) earthquake. The focal mechanisms of most of these events are strike-slip, as expected for transform faulting along the Pacific-North American plate boundary.

The seismicity in the GoC, north of the island Angel de la Guarda (Fig. 1), appears to occur in the form of large earthquake swarms, particularly near the Wagner ( $\sim 31^\circ \text{ N}$ ,  $114.1^\circ \text{ W}$ ) and upper Delfin ( $\sim 30.5^\circ \text{ N}$ ,  $113.9^\circ \text{ W}$ ) basins (Reichle and Reid, 1977). To the south of Canal de Ballenas, the plate boundary consists of well-defined en echelon transform zones. Goff *et al.* (1987) noted that the strike changes by about  $10^\circ$  between the dominantly oceanic Canal de Ballenas transform fault and the continental Cerro Prieto transform fault. They suggested that this change in strike

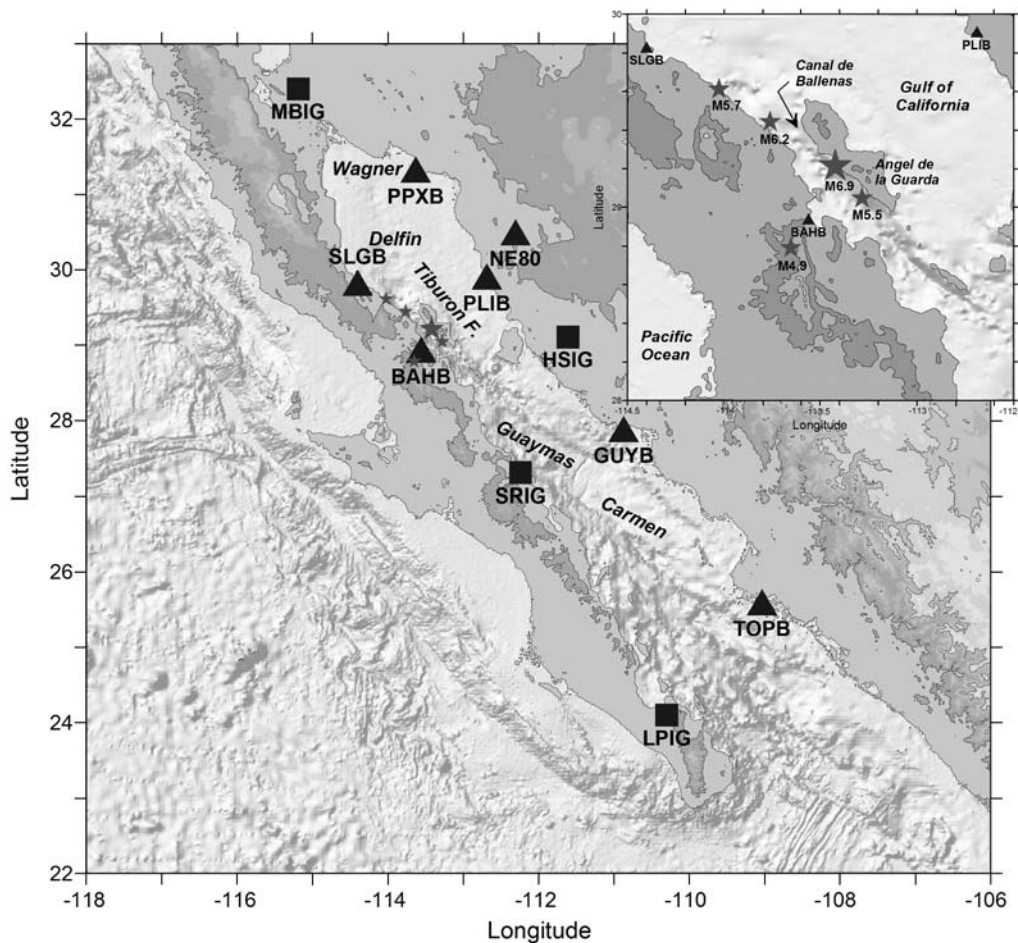


**Figure 1.** Map of the distribution of regional broadband stations that recorded the 2009 seismic sequence. The triangles are stations of the RESBAN array, operated by CICESE; the squares are the stations of the National Seismological Service, operated by UNAM. The stars are the initial locations of the main events that occurred on 3 August 2009, obtained with the regional body-wave arrivals and Hypoinverse (see also inset).

requires that the transition between oceanic and continental transform faults acts as a triple junction that allows compensating motion along a right-lateral, strike-slip fault trending more westerly than the Cerro Prieto fault.

On 3 August 2009 an earthquake of magnitude  $M_w$  6.9 occurred in the Canal de Ballenas region. The preliminary epicentral location reported by the National Seismological Service of Mexico [Servicio Sismológico Nacional (SSN)] and the Array Network Facility (ANF) suggested that the epicenter was on the North American plate in a zone where two major faults, the Tiburón and De Mar faults, are considered inactive (Aragón-Arreola and Martín-Barajas, 2007). This earthquake was preceded by a magnitude  $m_b$  5.5 event that occurred about 5 min before. In the next 40 min after the main event two aftershocks with magnitudes  $m_b$  4.9 and  $M_w$  6.2 occurred, and on 5 August a third aftershock of  $M$  5.5 was located in the Canal de Ballenas region. Because regional seismic stations in the GoC providing real time arrivals are sparse, the epicentral locations reported by worldwide networks are biased. For instance, Goff *et al.* (1987)

found that epicenters reported by the International Seismological Center are biased toward the north and east due to the concentration of stations in North America. Castro *et al.* (2007) and Castro, Pérez-Vertti, *et al.* (2010) compared epicentral locations reported in the Preliminary Determination of Epicenters (PDE) with locations obtained using regional arrival times and found that for events with magnitudes between 5 and 6.7, the discrepancy is on average about 25 km. We compare in Figure 3 our epicentral locations of the main events with the PDE locations (pluses) and the Global CMT catalog (open circles). The PDE location for the main event ( $M$  6.9) is offset by 55 km to the southeast. Although the centroid location does not have to necessarily coincide with the hypocenter, the Global CMT locations are close to our epicentral locations, particularly for the  $M$  6.2 aftershock.

The main event of this sequence is one of the few major earthquakes in the GoC instrumentally recorded. Pacheco and Sykes (1992) reported perhaps the largest earthquake in the GoC with  $M$  7.0, which occurred south of Carmen basin in 1901.

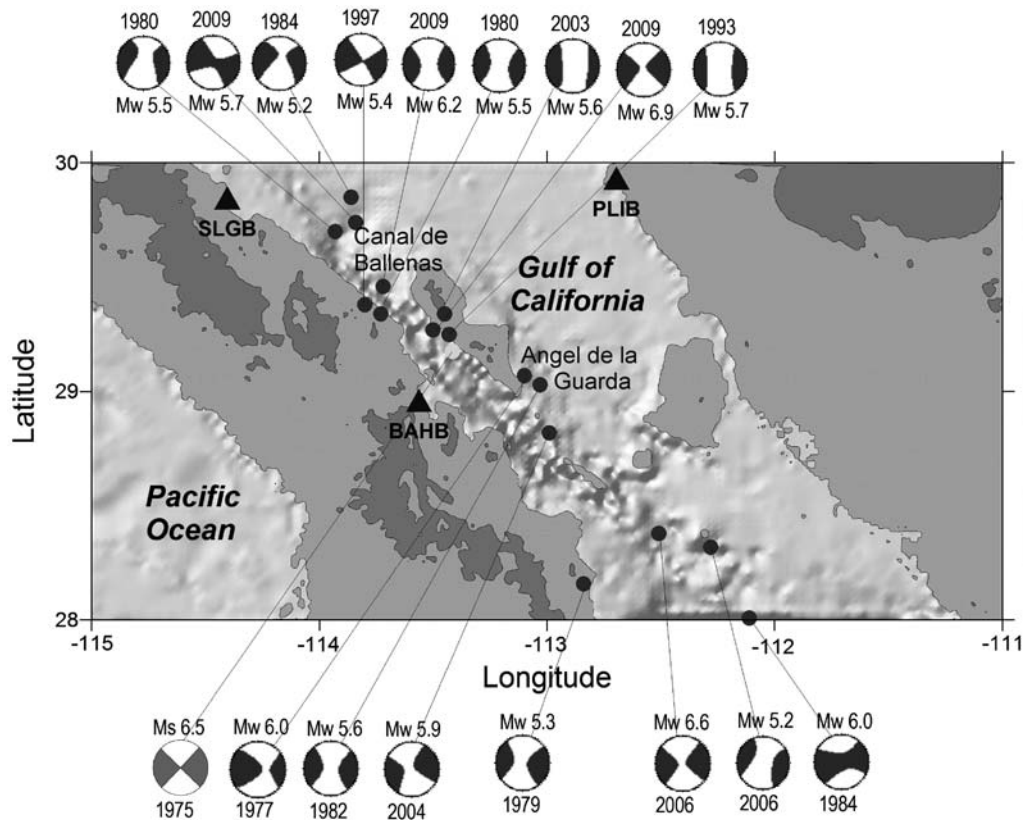


**Figure 2.** Centroid locations and focal mechanisms reported by the Global CMT catalog for the period 1976–2009. The focal mechanism of the 1975 event was obtained by Munguía *et al.* (1977), shown in gray. The triangles are broadband stations of the RESBAN seismic network.

Because of the variable bathymetry and crustal structure of the GoC, accurate epicentral locations are useful to conduct other studies such as body-waveform inversions (e.g., Goff *et al.*, 1987; Rebollar *et al.*, 2001; Abercrombie and Ekström, 2001, 2003; López-Pineda and Rebollar, 2005). In this study we determine precise epicentral locations of the August 2009 seismic sequence using  $P$ - and  $S$ -wave arrival times recorded by regional stations of the broadband network Red Sismológica de Banda Ancha (RESBAN) that Centro de Investigación Científica y de Educación Superior de Ensenada (CICESE) operates and by stations of the SSN located in the region of the GoC in La Paz, Hermosillo, Santa Rosalia, and Mexicali.

#### Data and Location of Epicenters

The stations of RESBAN consist of Guralp CMG-40T or CMG-3ESP sensors, 24-bit Guralp digitizers, a CMG-SAM2 acquisition module, and GPS for time control. The stations record continuously at 20 samples per second. The triangles in Figure 1 show the distribution of the seismic stations of this array. The stations of the SSN (squares in Fig. 1) consist of STS-2 triaxial sensors and 24-bit Quanterra digitizers. The data of these stations are sampled at 80–100 samples per second and transmitted via satellite, Internet, or telephone

to the data center located in the Instituto de Geofísica, Universidad Nacional Autónoma de México (UNAM) in México City. The events recorded by RESBAN are not located routinely, because the stations are autonomous, and small events ( $M < 3.5$ – $4.0$ ) in the GoC are not reported by the SSN. Thus, we started the analysis of the August 2009 seismic sequence by counting local events recorded by the closest station (BAHB) to Canal de Ballenas and to the preliminary epicentral locations of the main events (Fig. 1). Figure 4 shows the number of events recorded in Bahía de los Angeles (BAHB) with  $S$ - $P < 10$  s between 3 August 2009 and 5 August 2009. The sequence started on 3 August at 17:55 h (GMT) with an  $m_b$  5.5 earthquake, and the number of events increased after the main event ( $M_w$  6.9) that occurred at 18:00 h. Most of the events of the sequence occurred on 4 August, when another important aftershock with  $m_b$  4.1 was recorded. On 5 August (Fig. 4c) the last main aftershock with  $M_w$  5.7 occurred, and the number of earthquakes decreased considerably. To verify the duration of the sequence, we made an earthquake search in the U.S. Geological Survey earthquake data base from 1 August to 31 August 2009 in a rectangle with latitudes in the range of 28.5° to 30.0° N and longitudes in the range of 112.6° to 114.4° W; we found the events listed in Table 1. Note that for that region the PDE catalog reports only seven events in August 2009, all with  $M > 4.1$ .

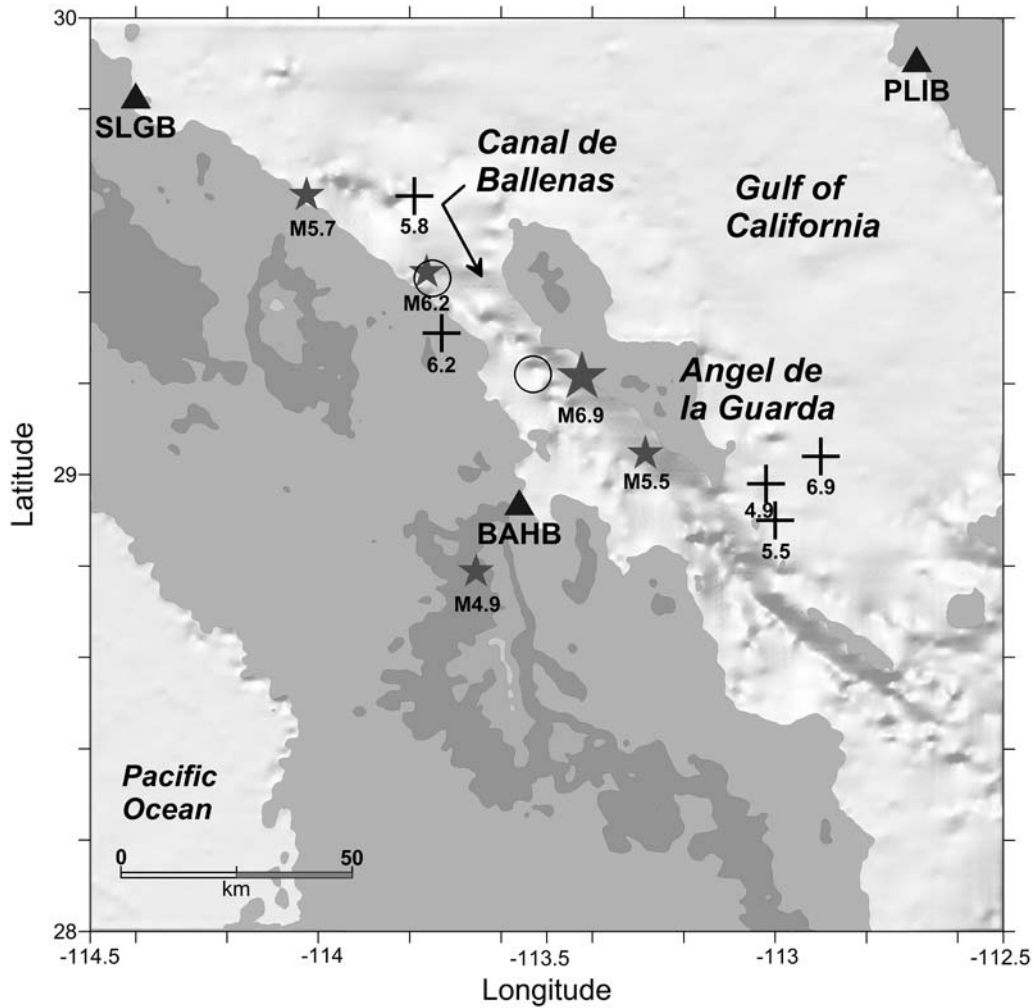


**Figure 3.** Map compares epicentral locations obtained from the regional broadband array (stars) with epicentral coordinates reported by PDE (crosses) and the centroid locations reported by the Global CMT catalog (open circles). The numbers indicate the magnitude of the event; the triangles indicate the stations.

To locate the aftershocks, we look for events recorded by at least three of the four regional stations shown in Figure 5 and with clear *P*- and *S*-wave arrivals. We determined a preliminary hypocentral location with the Hypoinverse code of Klein (2002) using at least four body-wave arrival times. We

adopted the velocity model proposed by González-Fernández *et al.* (2005), which is based on a 280-km-long profile run from the upper Tiburón basin (~29.3° N, 112.5° W) to the upper Delfín basin (~30.5° N, 114.8° W). This model consists of five layers. The uppermost sediments are represented by a

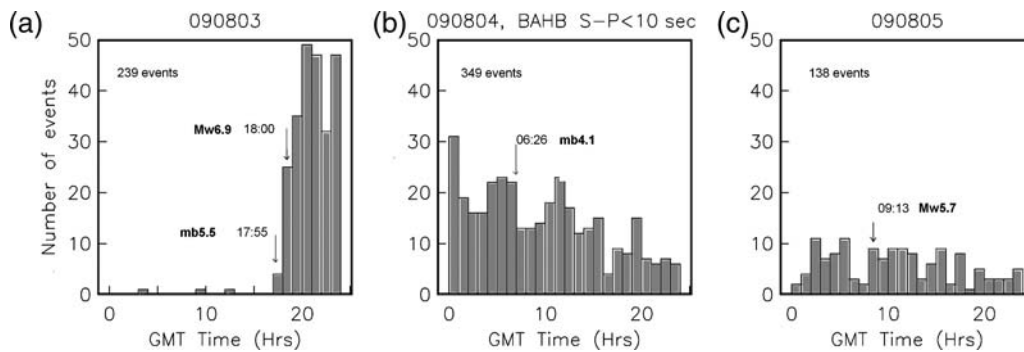


**Figure 4** Number of events recorded in Bahía de los Angeles (station BAHB) with *S-P* < 10 s. (a) 3 August 2009; (b) 4 August; (c) 5 August. The arrows indicate the time when the main events of the sequence occurred.

Table 1  
Earthquakes Reported in the PDE Catalog between 1 August and 31 August 2009, Located in the Canal de Ballenas Region (28.50°–30.00° N, 112.60°–114.40° W)

Date (yyyy/mm/dd)	Origin Time	Latitude °N	Longitude °W	Depth (km)	Magnitude
2009/08/03	17:55	28.90	113.00	10	5.5 $m_b$
2009/08/03	17:59	29.04	112.90	10	6.9 $M_w$
2009/08/03	18:07	29.05	113.12	10	4.9 $m_b$
2009/08/03	18:33	28.98	113.02	10	4.9 $m_b$
2009/08/03	18:40	29.31	113.73	10	6.2 $M_w$
2009/08/04	06:26	29.45	114.12	10	4.1 $m_b$
2009/08/05	09:13	29.61	113.79	10	5.7 $M_w$

2-km-thick layer with a  $P$ -wave velocity of 1.96 km/s. The second layer has a velocity of 4.6 km/s and a thickness of 6 km. The middle crust has a velocity of 5.52 km/s and the lower crust a velocity of 6.66 km/s. Below the Moho, at 24 km depth, the upper mantle has a velocity of 7.9 km/s and the half-space a velocity of 8.3 km/s, at depths greater than 55 km. Figure 5 shows the epicentral locations obtained with Hypoinverse and the regional arrival times. The stars are the epicentral locations of the main events, which are also listed in Table 2.

### Relocation Procedure

Because the seismicity associated with the main event of the sequence is distributed over a large area, we relocated the hypocenters dividing the aftershock region in the six boxes shown in Figure 5. We did this to minimize the travel-time perturbation produced by lateral variations of the velocity structure. We selected the number and position of the boxes based on the distribution of the initial epicentral locations. When possible we tried to separate events located in the

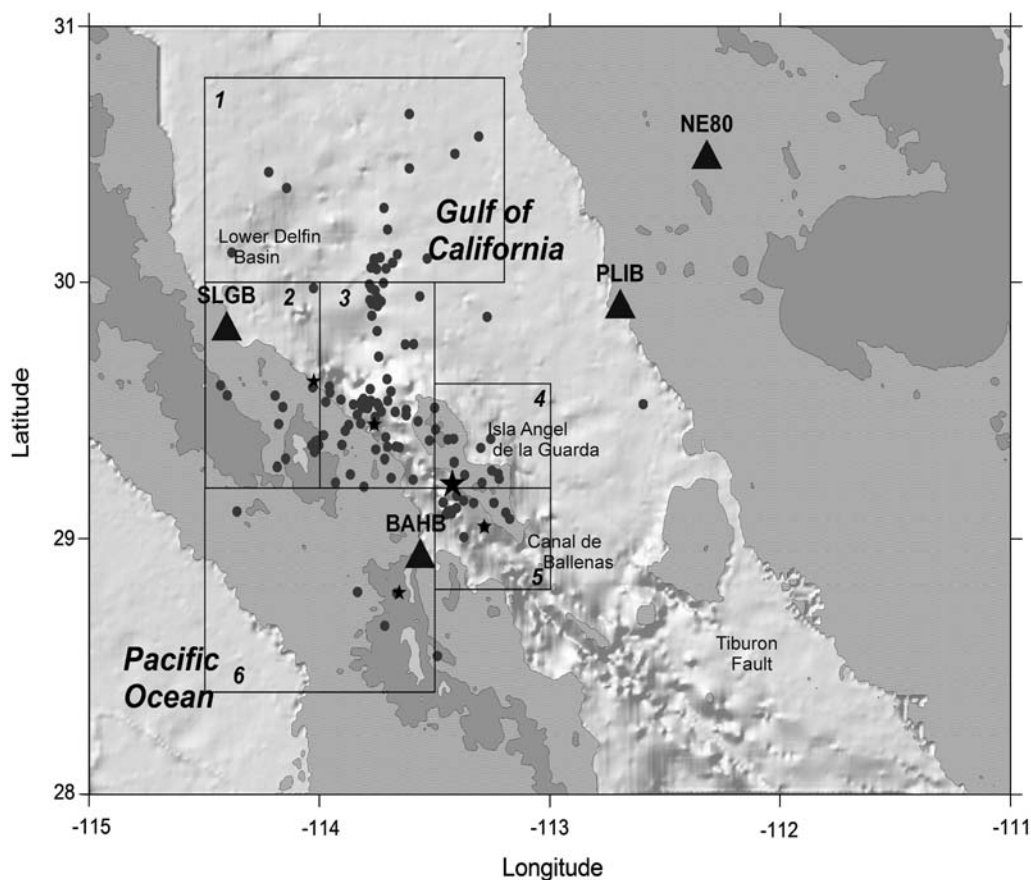


Figure 5. Initial locations obtained using the regional body-wave arrivals and Hypoinverse. For relocation purposes, we divided the region into six boxes. The stars are the main events of 3 August 2009.

**Table 2**  
 Preliminary Location of the Main Events of the Sequence Determined with Hypoinverse and Regional Arrival Times

Event	Date (yyyy/mm/dd)	Origin Time	Latitude °N	Longitude °W	Depth	Magnitude
000	2009/08/03	17:55	29.046	113.284	15.7	5.5 $m_b$
001	2009/08/03	17:59	29.214	113.423	1.9	6.9 $M_w$
002	2009/08/03	18:33	28.788	113.655	1.2	4.9 $m_b$
003	2009/08/03	18:40	29.443	113.763	4.6	6.2 $M_w$
004	2009/08/05	09:13	29.612	114.026	0.0	5.7 $M_w$

ocean from those located in the peninsular areas. For instance, boxes 1, 4, and 5 contain epicenters in the Gulf, while box 6 contains events located onshore. Although most events in box 2 are in the peninsula, the epicenters in box 3 are mixed. However, to calculate station corrections we restricted the events around the target event to be either oceanic or continental. We determined source-specific station terms (SSST), as proposed by Richards-Dinger and Shearer (2000)

to relocate the hypocenters. We used a modified version of the Comploc code of Lin and Shearer (2005) that uses regional phases ( $P_n$ ,  $P_g$ ,  $S_n$ ,  $S_g$ ) and weights the phase arrivals according to the corresponding source-station distance (e.g., Castro, Pérez-Vertti, et al., 2010; Castro, Shearer, et al., 2010). We used a velocity model with small gradients based on the velocity structure proposed by González-Fernández et al. (2005), because this model is representative of the

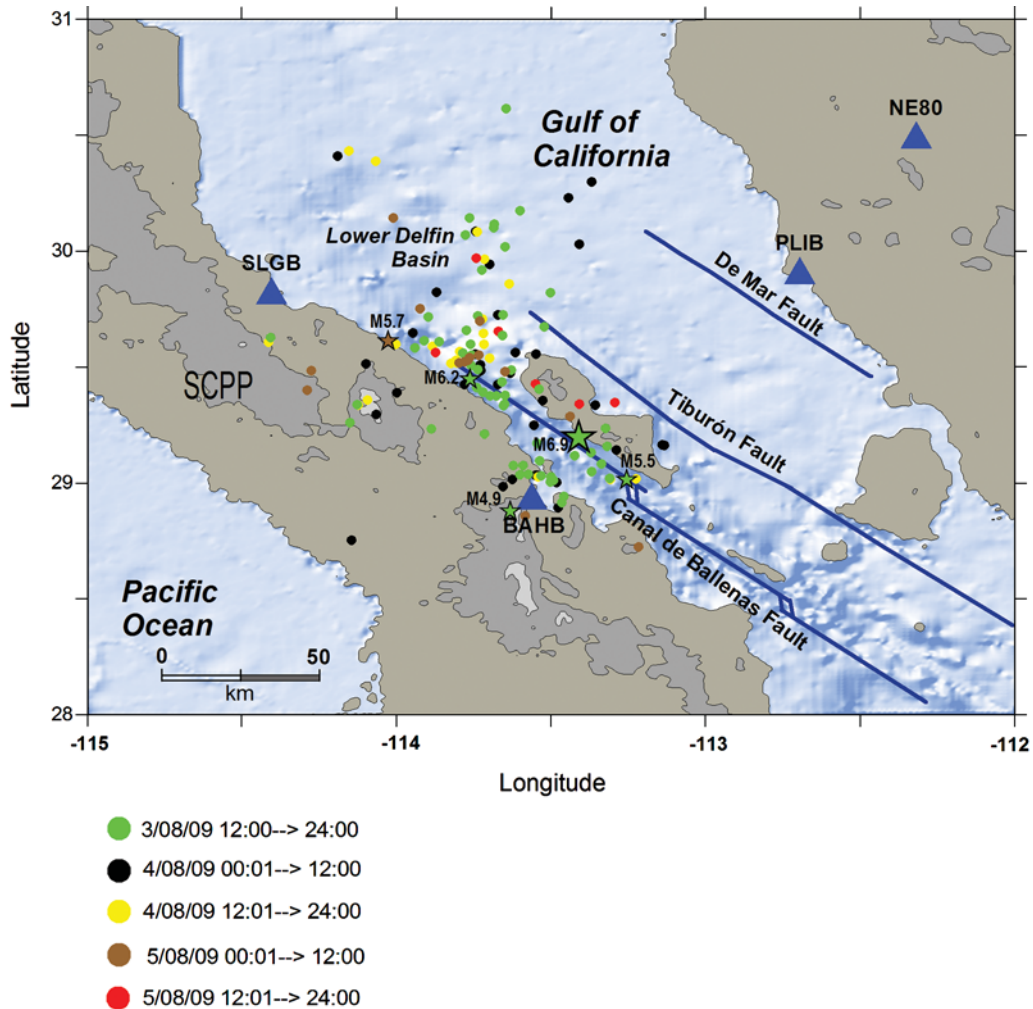


**Figure 6.** Distribution of epicenters relocated using the shrinking box source-specific station term (SSST) method of Lin and Shearer (2005). The stars are the epicenters of the main earthquakes, the numbers indicate the magnitudes and the triangles the recording stations. The traces of the faults were taken from Aragón-Areola and Martín-Barajas (2007).

region of our study and is similar to a model obtained by Phillips (1964) using active sources and sonobuoys. Figure 6 shows the epicenters relocated with the SSST method and the traces of the main faults, taken from Aragón-Arreola and Martín-Barajas (2007).

#### Location Uncertainties

We estimated the hypocentral uncertainties with a bootstrap approach similar to that described by Billings *et al.* (1994). We used the residuals at the best-fitting location for each event as an estimate of the picking errors. The residuals were randomly chosen from the total set for each event. The number of degrees of freedom in the location problem were taken into account by multiplying the residuals by the scaling factor  $n/(n-4)$ , where  $n$  is the number of picks. This technique was used by Shearer (1997) to estimate standard errors of the aftershock locations of the Whittier Narrows 1987 earthquake. In this approach the location uncertainties are based upon the scatter in the locations after repeating this process 200 times for each event. Figure 7a shows the average travel-time residuals of the best located events and the estimated standard errors (Fig. 7b,c for the horizontal and vertical errors, respectively). Seventy-eight percent of the events have horizontal errors  $ERH < 1$  km and 85% vertical errors  $ERZ < 1$  km.

To test the sensitivity of the location uncertainties to the chosen boxes, particularly box 3 that contains many events, we recalculated the hypocenters overlapping the areas of boxes 2 and 3 by 50% to the east and to the west, respectively. Figure 8a compares the travel-time errors (RMS1) of the events in box 2 before (Fig. 5) and after (RMS2) increasing the width of the box 50% to the east. A similar calculation was made for the events in box 3 by also increasing the width 50%, but to the west (Fig. 8b). In both cases the RMS values do not change very much, indicating that the exact boundaries of the boxes do not have much effect on the estimated errors in hypocentral location.

## Results and Discussion

Eighty-seven percent of the best located events of the sequence ( $RMS < 1.0$  s) (Fig. 6) have an average residual less than 0.4 s (Fig. 7a). Many of the aftershocks are located along the Canal de Ballenas transform fault, particularly at the northern end. The sequence started at the southern end of the channel with the  $m_b$  5.5 foreshock. Then the main event ( $M_w$  6.9) occurred 25 km northeast, triggering events on the Canal de Ballenas fault and on local faults near Bahia de los Angeles, including the  $m_b$  4.9 aftershock located southwest of BAHB (Fig. 6). Forty minutes after the main event, the  $M_w$  6.2 aftershock occurred in Canal de Ballenas and the seismicity migrated to the northwestern end of the fault where the last main aftershock with  $M_w$  5.7 occurred. It is interesting to note that the aftershocks tended to concentrate on the northwestern end of the fault, where three topographic highs seem to form a barrier (see Figs. 1, 3, and 6), beyond which the seismicity is absent. At that point the aftershocks (yellow to red dots in Fig. 6) migrated north toward the lower Delfin basin ( $\sim 29.9^\circ$  N,  $113.8^\circ$  W). We also located several earthquakes south and west of the  $M_w$  5.7 aftershock in the Stable Central Peninsula Province (SCPP) in Figure 6, which is characterized by the absence of deformation related with the extension of the Gulf (Stock *et al.*, 1991). These events can be considered intraplate events resulting from the stress transfer generated during the rupture of the plate boundary along the Canal de Ballenas fault. While most events of the sequence are located between the Tiburón fault and the Canal de Ballenas fault (Fig. 6), the seismicity is absent between the Tiburón and De Mar faults. Aragón-Arreola and Martín-Barajas (2007) interpreted a seismic line that crosses the upper Tiburón basin and those two faults; they found that the region between Tiburón and De Mar faults is structurally inactive.

To estimate the rupture area we measured the distance between the epicenter of the main event and the northern end of the Canal de Ballenas fault, as mapped by Aragón-Arreola and Martín-Barajas (2007), to obtain a rupture length  $L = 50$  km. Then, using a fault width  $W = 12$  km, based

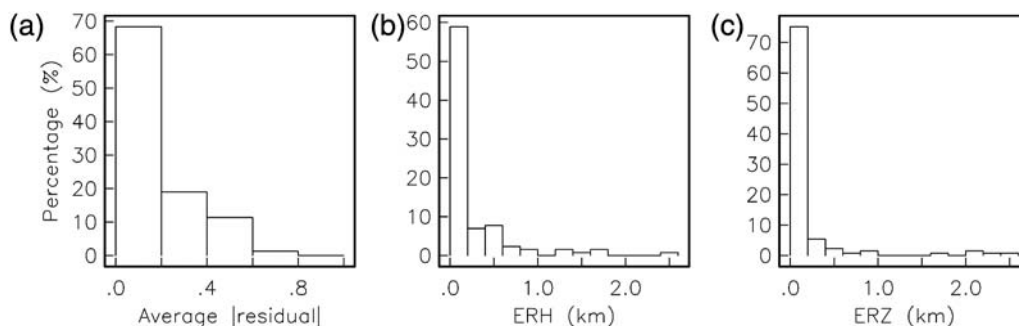


**Figure 7.** Histograms of location uncertainties: (a) the average absolute value of the travel-time residuals; (b) the estimated horizontal errors; and (c) the vertical errors. The residuals correspond to the SSST relocations based on the velocity model proposed by González-Fernández *et al.* (2005) for the upper Gulf of California. The horizontal (ERH) and vertical (ERZ) errors were estimated with a bootstrap approach described in the text.

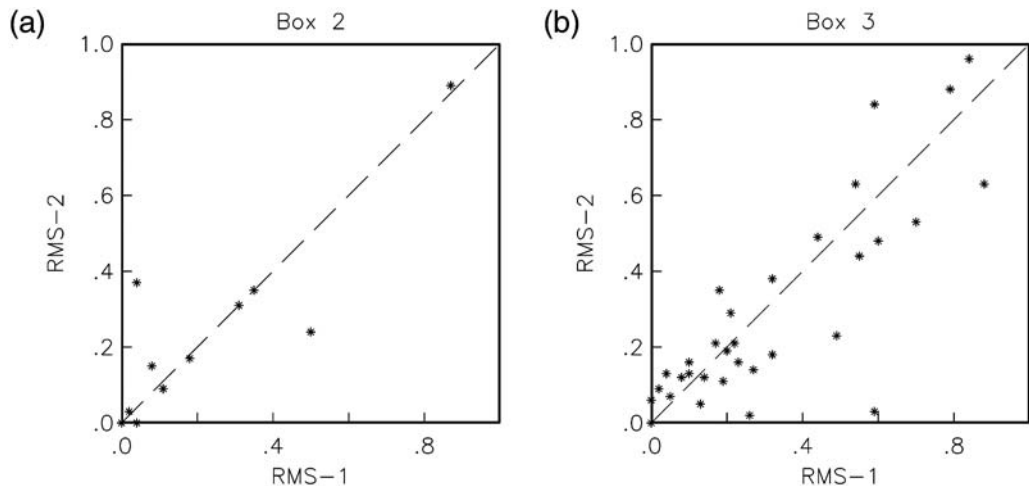


**Figure 8.** Comparison of travel-time root mean square values: (a) events in box 2 of Figure 5 (RMS1) versus the rms values recalculated by increasing the width of that box 50% to the east; and (b) event in box 3, as in Figure 5 (RMS1) and after increasing the width of that box 50% to the west (RMS2).

on the aftershock depth distribution (Fig. 9), we estimate a rupture area  $A = 600 \text{ km}^2$ . Note in Figure 9 that the fault width could be greater because there are aftershocks deeper than 12 km. However, the assumed fault width of 12 km is

also based on the hypocentral distribution of the previous 1975 earthquake sequence. Munguía *et al.* (1977) found that the aftershocks of the 1975 Canal de Ballenas earthquakes were located up to 10–15 km deep. The rupture area thus

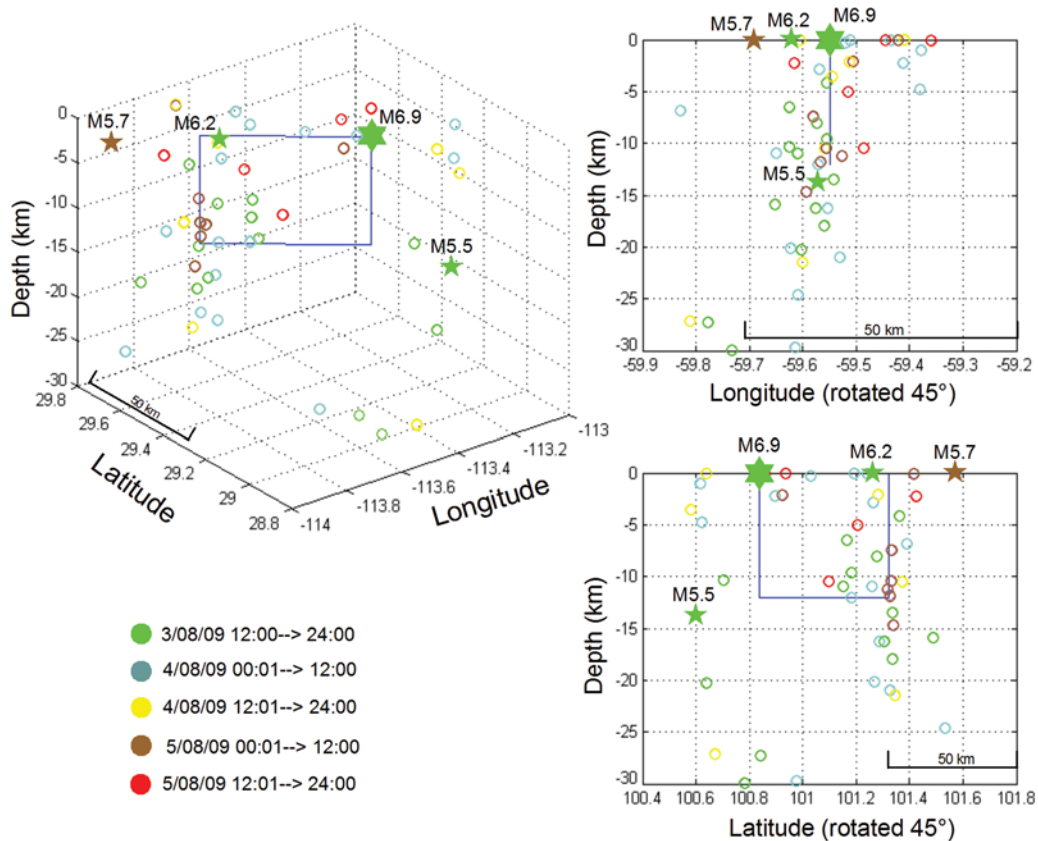


**Figure 9.** Distribution of focal depths of the best located aftershocks inside boxes 3, 4, and 5 (Figs. 5 and 6). The straight lines represent the Canal de Ballenas fault plane in a 3D plot (left) and cross sections (plots on the right side). On top is a cross-section perpendicular to the fault plane and on the bottom a cross section in the direction of the fault plane. The stars are the locations of the main event relative to the fault plane.

calculated is consistent with the expected area from the Wells and Coppersmith (1994) regression equation for an  $M_w$  6.8 strike-slip earthquake. Using the seismic moment  $M_0 = 2.59 \times 10^{26}$  dyne · cm, reported in the Global CMT catalog, we made a rough estimate of 1.3 m for the average fault displacement, and a stress drop  $\Delta\sigma = 2.2$  MPa using the relation  $\Delta\sigma = \frac{2}{\pi W} \frac{M_0}{A}$  for a strike-slip fault (Lay and Wallace, 1995). The aftershock distribution (Fig. 6) suggests that the rupture may have started in the southern end of the fault where the  $m_b$  5.5 foreshock was located, terminating beyond the northern end of the fault where the  $M_w$  5.7 aftershock occurred. Under this assumption, we can estimate the upper limit of the rupture area by setting  $L = 100$  km and  $W = 14$  km (based on the focal depth of the foreshock, 13.7 km) to obtain  $A = 1400$  km<sup>2</sup> and  $\Delta\sigma = 0.8$  MPa. To estimate the lower limit of the rupture area we can use the distance between the main event and the  $M$  6.2 aftershock (see lower frame of Fig. 9) to obtain  $L = 43$  km. Then, if we only use aftershocks that occurred on 3 August (green circles in Fig. 9), we can define  $W = 10$  km and a rupture area  $A = 430$  km<sup>2</sup> to estimate  $\Delta\sigma = 3.7$  MPa.

For the July 1975 Canal de Ballenas earthquake ( $M_s = 6.5$ ), Munguía *et al.* (1977) estimated a stress drop of 0.4 MPa. The low stress drop of this event, and that obtained by us for the 2009 earthquake (2.2 MPa), contrasts with a recent investigation of Allmann and Shearer (2009) on the global variation of earthquake stress drop. They observed higher stress drops for strike-slip earthquakes and higher median stress drop values (6.0 MPa) for oceanic transform fault (OTF) events, compared with interplate events (3.3 MPa). The low stress drops obtained for the 1975 and 2009 Canal de Ballenas earthquakes may be due to the long rupture duration compared to their seismic moment, as suggested in previous studies of OTF events (Beroza and Jordan, 1990; McGuire *et al.*, 1996). Slow OTF earthquakes may result in low apparent stresses due to depletion in higher frequencies (Kanamori and Stewart, 1976; Stein and Pelayo,

1991; Shearer, 1994; Pérez-Campos *et al.*, 2003; Allmann and Shearer, 2009). For instance, Kanamori and Stewart (1976) found that along the Gibbs fracture zone, at least two large earthquakes (in 1967 and 1974) involve a slow fracture process. This, together with the large fault length estimated, explains the low high-frequency energy radiated by these earthquakes and the disparity observed between  $m_b$  and  $M_s$ , between  $M_s$  and seismic moment, and the low apparent stresses. Other early papers on ocean transform fault earthquakes (e.g., McGuire *et al.*, 1996) have also proposed that these events have a slow rupture component. However, these early observations are controversial because more recent studies (Abercrombie and Ekström, 2001, 2003) show that some of the proposed slow rupture components previously found on oceanic transform faults are an artifact of modeling assumptions.

To analyze the distribution of focal depths relative to the Canal de Ballenas transform fault, we plot in Figure 9 the relocated hypocenters of events in boxes 3, 4, and 5 (Figs. 5 and 6). The rectangle in Figure 9 represents the northern segment of the Canal de Ballenas fault taken from Aragón-Arreola and Martín-Barajas (2007) and reproduced in Figure 6. The bigger star in Figure 9 is the location of the main event; the smaller stars are events with  $M \geq 5.5$  listed in Table 2. On the right side of Figure 9 are cross sections perpendicular to the fault (top frame) and along the fault plane (bottom frame). The foreshock that started the rupture is located at 13.7 km depth on the southeastern corner of the fault plane. The rupture propagated up and northwest, triggering the main event at a shallow depth. Then, the aftershocks concentrated on the northwestern edge of the fault with foci distributed at various depths between 0 and about 20 km. The last main aftershock of the sequence, located on the northwestern end of the fault (small star) is near two seamounts that seem to mark the northern end of the Canal de Ballenas fault. Figure 10 shows how the foci are distributed with depth within the Gulf of California and in the Baja

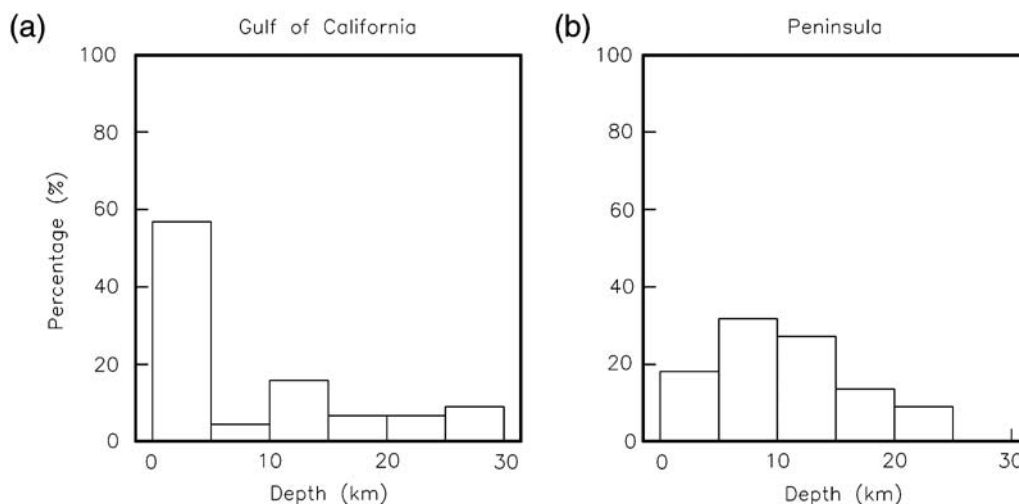


**Figure 10.** Histograms of focal depths of the events located in (a) the Gulf of California and in (b) the Peninsula de Baja California.

California peninsula. While events located in the GoC (Fig. 10a) are mostly shallow events, 57% with depths  $h \leq 5$  km and 77% with  $h \leq 15$  km, the aftershocks located inside the peninsula (Fig. 10b) tend to have deeper hypocenters (73% with  $h = 5$ –20 km). Several authors (Wiens and Stein, 1983, 1984; Bergman and Solomon, 1984) have observed that in young oceanic lithosphere the centroid depths can extend to the depth of the 800°C isotherm. Along transform faults, this isotherm is reached at depths between 6 and 10 km (Goff *et al.*, 1987). Abercrombie and Ekström (2001) found that the 600°C isotherm gives a good estimate of the limit of seismic slip, which is cooler than previous estimates for transform fault events. In the GoC, Goff *et al.* (1987) found that subevents tend to have centroid depths of 12–15 km and for normal faulting earthquakes between 3 and 6 km, particularly in the northern GoC. They also concluded that centroid depths for most strike-slip events in the GoC can be anywhere from immediately beneath the seafloor to approximately 10 km below and sometimes deeper. The median focal depths of the 2009 Canal de Ballenas sequence (Fig. 10a) are consistent with that interpretation.

### Summary and Conclusions

We used regional body-wave arrivals recorded by broadband stations located around the GoC to locate the earthquakes that occurred between 3 August and 5 August 2009 in the north-central region of the Gulf. Then, we relocated the hypocenters using the SSST method (Lin and Shearer, 2005) and found that the main event of 3 August 2009 ( $M_w$  6.9) and the bigger aftershocks of the sequence ( $M > 5.4$ ) occurred on the Canal de Ballenas fault, along the boundary between the Pacific and the North American plates. The main event of the sequence is the biggest earthquake ever recorded instrumentally on the Canal de Ballenas transform fault (Fig. 2). Before this event, on 8 July 1975 an  $M_s$  6.5 earthquake occurred approximately in the same location, where the fault had been locked for at least 20 years (Munguía *et al.*, 1977). The relocated events (Fig. 6) correlate better with the faults of the region and form more planar features than the preliminary epicenters (Fig. 5).

The 2009 earthquake sequence started south of Canal de Ballenas fault with an  $m_b$  5.5 foreshock and finished in the northwestern end of the fault with an  $M_w$  5.7 aftershock. The spatial distribution of the aftershocks indicates that the length of fault rupture is approximately 50 km. We assumed a fault width of 12 km, based on the aftershock focal depth distribution, to estimate a rupture area of 600 km<sup>2</sup>, an average slip of 1.3 m, and a stress drop of 2.2 MPa.

### Data and Resources

The seismograms used in this paper were recorded by stations of the RESBAN seismic array and the SSN. Data from the RESBAN and SSN networks can be requested from the first and second authors of this paper, respectively. Some

plots were made using the Generic Mapping Tools ([www.soest.hawaii.edu/gmt](http://www.soest.hawaii.edu/gmt), last accessed May 2010; Wessel and Smith, 2009).

### Acknowledgments

The operation of the RESBAN array has been possible thanks to the financial support of the Mexican National Council for Science and Technology (CONACYT) by means of the project 48852. Part of the analysis of this paper was made while one of the authors (RRC) was a UC MEXUS-CONACYT Visiting Scholar at the University of California, San Diego, IGPP-SIO. We also thank Luis Inzunza for the technical support provided, and the technicians of the SSN for supporting and maintaining the stations. SSN stations, except in the region of the GoC in La Paz, have been financially supported by the Mexican Department of Interior. We are thankful for the comments and suggestions provided by associate editor Cezar Trifu, and the reviews by Rachel Abercrombie and an anonymous reviewer.

### References

- Abercrombie, R. E., and G. Ekström (2001). Earthquake slip on oceanic transform faults, *Nature* **410**, 74–77.
- Abercrombie, R. E., and G. Ekström (2003). A reassessment of the rupture characteristics of oceanic transform earthquakes, *J. Geophys. Res.* **108**, 2225, doi [10.1029/2001JB000814](https://doi.org/10.1029/2001JB000814).
- Allmann, B. P., and P. M. Shearer (2009). Global variations of stress drop for moderate to large earthquakes, *J. Geophys. Res.* **114**, B01310, doi [10.1029/2008JB005821](https://doi.org/10.1029/2008JB005821).
- Aragón-Areola, M., and A. Martín-Barajas (2007). Westward migration of extension in the northern Gulf of California, Mexico, *Geology* **35**, 571–574.
- Bergman, E. A., and S. C. Solomon (1984). Source mechanisms of earthquakes near mid-ocean ridges from body waveform inversion: Implications for the early evolution of oceanic lithosphere, *J. Geophys. Res.* **89**, 11,415–11,441.
- Billings, S. D., M. S. Sambridge, and B. L. N. Kennett (1994). Errors in hypocenter location: Picking, model, and magnitude dependence, *Bull. Seismol. Soc. Am.* **84**, 1978–1990.
- Beroza, G., and T. Jordan (1990). Searching for show and silent earthquakes using free oscillations, *J. Geophys. Res.* **95**, 2485–2510.
- Castro, R. R., I. Mendez, A. Pérez-Vertti, A. Mendoza, and L. Inzunza (2007). Seismicity in the Gulf of California region recorded by the NARS-Baja array: Preliminary results, *Eos Trans. AGU* **88**, no. (23) Jt. Assem. Suppl., Abstract S31A-08.
- Castro, R. R., A. Pérez-Vertti, I. Mendez, A. Mendoza, and L. Inzunza (2010). Location of moderate-sized earthquakes recorded by the NARS-Baja array in the Gulf of California region between 2002 and 2006, *Pure Appl. Geophys.*, doi [10.1007/s00024-010-0177-y](https://doi.org/10.1007/s00024-010-0177-y)
- Castro, R. R., P. M. Shearer, L. Astiz, M. Suter, C. Jacques-Ayala, and F. Vernon (2010). The long-lasting aftershock series of the 3 May 1887  $M_w$  7.5 Sonora earthquake in the Mexican Basin and Range Province, *Bull. Seismol. Soc. Am.* **100**, 1153–1164.
- Goff, J. A., E. A. Bergman, and S. C. Solomon (1987). Earthquake source mechanism and transform fault tectonics in the Gulf of California, *J. Geophys. Res.* **92**, 10,485–10,510.
- González-Fernández, A., J. J. Dañobeitia, L. A. Delgado-Argote, F. Michaud, D. Córdoba, and R. Bartolomé (2005). Mode of extension and rifting history of upper Tiburón and upper Delfín basins, northern Gulf of California, *J. Geophys. Res.* **110**, B01313, doi [10.1029/2003JB002941](https://doi.org/10.1029/2003JB002941).
- Kanamori, H., and G. Stewart (1976). Mode of strain release along the Gibbs fracture zone, Mid-Atlantic Ridge, *Phys. Earth Planet. Inter.* **11**, 312–332.
- Klein, F. W. (2002). User's guide to HYPOINVERSE-2000, a Fortran program to solve for earthquake locations and magnitudes, *USGS Open File Report 02-171*, 121 pp.

- Lay, T., and T. C. Wallace (1995). *Modern Global Seismology*, Academic Press, New York, 521 pp.
- Lin, G., and P. M. Shearer (2005). Tests of relative earthquake location techniques using synthetic data, *J. Geophys. Res.* **110**, B04304, doi [10.1029/2004JB003380](https://doi.org/10.1029/2004JB003380).
- Lizarralde, D., G. J. Axen, H. E. Brown, J. M. Fletcher, A. González-Fernández, A. J. Harding, W. S. Holbrook, G. M. Kent, P. Paramo, and F. Sutherland (2007). Variation in styles of rifting in the Gulf of California, *Nature* **448**, doi [10.1038/nature06035](https://doi.org/10.1038/nature06035).
- Lonsdale, P. L. (1989). Geology and tectonics history of the Gulf of California, in *The Geology of North America* vol. N, Geological Society of America, Boulder, Colorado.
- López-Pineda, L., and C. J. Rebolgar (2005). Source characteristics of the  $M_w$  2 Loreto earthquake of 12 March 2003 that occurred in a transform fault in the middle of the Gulf of California, Mexico, *Bull. Seismol. Soc. Am.* **95**, 419–430.
- McGuire, J., P. Ihmle, and T. Jordan (1996). Time-domain observations of a slow precursor to the 1994 Romanche transform earthquake, *Science* **274**, 82–85.
- Molnar, P. (1973). Fault plane solutions of earthquakes and direction of motion in the Gulf of California and on the Rivera fracture zone, *Geol. Soc. Am. Bull.* **84**, 1651–1658.
- Munguía, L., M. Reichle, A. Reyes, R. Simona, and J. Brune (1977). Aftershocks of the 8 July, 1975 Canal de las Ballenas, Gulf of California, earthquake, *Geophys. Res. Lett.* **4**, 507–509.
- Pacheco, J. F., and L. R. Sykes (1992). Seismic moment catalog of large shallow earthquakes, 1900 to 1989, *Bull. Seismol. Soc. Am.* **82**, 1306–1349.
- Pérez-Campos, X., J. McGuire, and G. Beroza (2003). Resolution of the slow earthquake/high apparent stress paradox for oceanic transform fault earthquakes, *J. Geophys. Res.* **108**, no. B9, 2444, doi [10.1029/2002JB002312](https://doi.org/10.1029/2002JB002312).
- Phillips, R. P. (1964). Seismic refraction studies in the Gulf of California, in *Marine Geology of the Gulf of California*, edited by T. H. Van Andel and G. G. Shor (Editors), AAPG Mem., 3, 90–121.
- Rebolgar, C. J., L. Quintanar, R. R. Castro, S. M. Day, J. Madrid, J. N. Brune, L. Astiz, and F. Vernon (2001). Source characteristics of a 5.5 magnitude earthquake that occurred in the transform fault system of the Delfin Basin in the Gulf of California, *Bull. Seismol. Soc. Am.* **91**, 781–791.
- Reichle, M., and I. Reid (1977). Detailed study of earthquake swarms from the Gulf of California, *Bull. Seismol. Soc. Am.* **67**, 159–171.
- Richards-Dinger, K., and P. Shearer (2000). Earthquake locations in southern California obtained using source-specific station terms, *J. Geophys. Res.* **105**, 10,939–10,960.
- Rodríguez-Lozoya, H. E., L. Quintanar, R. Ortega, C. J. Rebolgar, and Y. Yagi (2008). Rupture process of four medium-sized earthquakes that occurred in the Gulf of California, *J. Geophys. Res.* **113**, B10301, doi [10.1029/2007JB005323](https://doi.org/10.1029/2007JB005323).
- Shearer, P. (1994). Global seismic event detection using a matched-filter on long-period seismograms, *J. Geophys. Res.* **99**, 13,713–13,725.
- Shearer, P. (1997). Improving local earthquake locations using the L1 norm and waveform cross correlation: Application to the Whittier Narrows, California, aftershock sequence, *J. Geophys. Res.* **102**, 8269–8283.
- Stein, S., and A. Pelayo (1991). Seismological constraints on stress in the oceanic lithosphere, *Philos. Trans. R. Soc. London, Ser. A* **337**, 53–72.
- Stock, J. M., A. Martín-Barajas, F. Suárez-Vidal, and M. M. Miller (1991). Miocene to Holocene extensional tectonics and volcanic stratigraphy of the northeastern Baja California, México, in *Geological Excursions in the Southern California and México*, M. J. Walawender and B. B. Hanan (Editors), 44–67, Geol. Soc. Am., Boulder, Colorado.
- Wells, D. L., and K. J. Coppersmith (1994). New empirical relationships among magnitude, rupture length, rupture width, rupture area, and surface displacement, *Bull. Seismol. Soc. Am.* **84**, 974–1002.
- Wessel, P., and W. H. F. Smith (2009). *The Generic Mapping Tools (GMT) version 4.5.0 Technical Reference & Cookbook*, SOEST/NOAA.
- Wiens, D. A., and S. Stein (1983). Age dependence of oceanic intraplate seismicity and implications for lithosphere evolution, *J. Geophys. Res.* **88**, 6455–6468.
- Wiens, D. A., and S. Stein (1984). Intraplate seismicity and stresses in young oceanic lithosphere, *J. Geophys. Res.* **89**, 11,442–11,464.
- Centro de Investigación Científica y de Educación Superior de Ensenada (CICESE)  
División Ciencias de la Tierra  
Departamento de Sismología, km 107 Carretera Tijuana-Ensenada  
22860 Ensenada  
Baja California, México  
(R.R.C., V.W., A.P., A.M.)
- Servicio Sismológico Nacional  
Instituto de Geofísica  
Universidad Nacional Autónoma de México (UNAM)  
Ciudad Universitaria, México  
(C.V.)
- Institute of Geophysics and Planetary Physics  
Scripps Institute of Oceanography  
University of California–San Diego  
La Jolla, California 92093-0225  
(P.S., L.A., F.V.)